167 (2022) 207244

Contents lists available at ScienceDirect

Micro and Nanostructures

journal homepage: www.journals.elsevier.com/micro-and-nanostructures

Engineering the band gap of BN and BC_2N nanotubes based on T-graphene sheets using a transverse electric field: Density functional theory study

Roya Majidi [a,*], Ahmad I. Ayesh [b]

[a] Department of Physics, Shahid Rajaee Teacher Training University, Lavizan, 16788-15811, Tehran, Iran
[b] Department of Mathematics, Statistics and Physics, Qatar University, P. O. Box 2713, Doha, Qatar

ARTICLE INFO

Keywords:
Nanotube
T-graphene
Electronic properties
BN
BC_2N
DFT

ABSTRACT

A new class of nanotubes formed by rolling boron nitride (BN) and boron carbonitride (BC_2N) sheets in the form of T-graphene is suggested in this work. The structural and electronic properties of these nanotubes, named T-BNNTs and T-BC_2NNTs, are systematically studied by density functional theory (DFT) calculations. The tubes with different chirality and size are considered. Their structural stability is evaluated by calculation of cohesive energy and ab-initio molecular dynamics simulation. The results confirm the thermal stability of the considered T-BNNTs and T-BC_2NNTs. The calculated electronic band structures and density of states reveal that the T-BNNTs are insulators, independent of their size and chirality. The T-BC_2NNTs show both metallic and semiconducting properties. Our results indicate that the electronic properties of T-BNNTs and T-BC_2NNTs can be successfully tuned by applying an external electric field, which makes the application of these tubes in nanoelectronic devices more promising.

1. Introduction

The discovery of graphene, a two-dimensional (2D) layer honeycomb structure composed of carbon atoms [1], has drawn incredible attention. Graphene has promising applications in numerous fields such as electronics, photonics, optoelectronics, energy storage, etc. [2–5] due to its special structure and inherent extraordinary properties [6–8]. In particular, the special electronic band structure with Dirac points and cones gives graphene massless fermions which leads to quantum Hall effects, ultra-high carrier mobility, and magnetoelectric effects in topological materials [9–13]. Inspired by the huge success of graphene, rigorous attention was focused on experimental and theoretical studies of other 2D carbon-like structures including graphyne as well as T-, R-, S-, penta-, and pha-graphene [14–20]. These sheets with non-hexagonal structures show various electronic properties.

Apart from the carbon-based monolayers, researchers investigated different non-carbon-based 2D materials. Since B, N, Si, and Ge atoms are the nearest neighbors of the C atom in the periodic table; various sheets prepared by fusion of these atoms have been investigated. For instance, boron nitride (BN) sheets with a hexagonal structure similar to graphene were proposed [21–23]. The single-layer of BN sheets are composed of alternating B and N atoms in a honeycomb organization comprising of sp^2-bonded 2D layers [23]. Despite structural similarities, graphene-like BN sheets show physical and chemical features that are significantly distinct from graphene sheets because of the ionic properties of B–N bonds. In contrast to semimetallic property of graphene, a hexagonal BN sheet is

* Corresponding author.
E-mail addresses: royamajidi@gmail.com, r.majidi@sru.ac.ir (R. Majidi).

https://doi.org/10.1016/j.micrna.2022.207244
Received 4 January 2022; Received in revised form 29 April 2022; Accepted 4 May 2022
Available online 10 May 2022

a semiconductor with a wide band gap [23–26]. However, the zero band gap of graphene and the wide band gap of the graphene-like BN sheets are a major limitation against implementing these materials for electronic devices based on semiconductors. Hence, substantial effort is needed to find semiconductors with band gap energies intermediate between graphene and BN sheets. For example, graphene-like sheets composed of different numbers of B, N, and C atoms have been identified as promising candidates for nanoelectronics [27–31]. These 2D materials display diverse electronic properties ranging from semimetallic to semiconducting depending on their composition of C, B, and N atoms within the atomic lattice. The BN and BCN sheets with tetrarings, called T-graphene like sheets, have been investigated following the prediction of T-graphene sheets [32,33]. In contrast to T-graphene with semimetallic properties, T-graphene like BCN and BN sheets reveal semiconducting characteristics. Hence, these sheets may be utilized for electronic devices based on semiconductors.

Besides graphene and graphene-like 2D materials, one-dimensional (1D) tubes have also attracted widespread interest [34–38]. Nanotubes with different diameters can be built by cutting part of a 2D sheet and rolling it. In particular, carbon nanotubes (CNTs) based on graphene sheets have been developed as feasible materials with various properties to be used for gas sensors, hydrogen storage, textiles, and many more [35–39]. Here, C atoms are arranged in the honeycomb grids on the surface of CNTs. BN nanotubes (BNNTs) with similar atomic structure as CNTs have been also emerged [40–43]. The dynamical stability of BNNTs is confirmed by calculations of phonon dispersion [44]. While CNTs can have metallic or semiconducting properties depending on their chirality and diameter, all BNNTs are materials with a large band gap of around 5.5 eV which is independent of the tube diameters, chirality, and the number of walls [42]. The independent band gap to the tube geometry is a noteworthy advantage of BNNTs in comparison with CNTs. However, the wide band gaps of BNNTs severely restrict their applications. Thus, finding approaches to tune the band gap of BNNTs is essential. It was shown that this band gap can be decreased by doping [45–47].

Up to now, researchers have predicted and synthesized several ternary boron carbonitride (BCN) nanotubes [46–51]. The BC2N is understood to be the most stable form of the ternary tubes. These tubes have electronic properties between BNNTs as a semiconductor material and CNTs whose properties are dependent on the chirality and diameter of the tube [51]. The applications of BNNTs and BCNNTs have been established based on their properties, not found on CNTs. The results show the possibility of using BNNTs as drug carriers, sensors, high-capacity energy storage medium, transistors, and switches [52].

Furthermore, there have been several efforts seeking a novel set of nanotubes rolled from sheets such as graphyne, graphenylene, S-graphyne, T-graphene, etc. [53–59]. For instance, the computational study of the structural, optical, electronic, and thermoelectric properties of T-graphene nanotubes (T-CNTs) was reported recently [59]. The results revealed that rolling up a T-graphene sheet into a nanotube required less energy than rolling up a graphene sheet to form conventional CNTs. This implies the beneficial stability of T-CNTs. It was also shown that these nanotubes have metallic or semimetallic properties, and their number of Dirac points increased with increasing the tube diameter [59,60]. Recently, BN nanotubes composed of four-and eight-membered rings, referred to as T-BNNTs, have been simulated [61]. The electronic properties of the considered T-BNNTs showed that these BN nanotubes have a smaller band gap compared to BNNTs [61]. Hence, T-BNNTs have the band gaps, which fully conformed to the band gap required for the third generation of semiconductor nanomaterials, i.e. more than 2.5 eV [61].

Motivated by these results, we have proposed new BC_2N nanotubes that exhibit T-graphene like structures named T-BC_2NNTs in the present work. The structural and electronic properties of T-BC_2NNT are studied and compared with T-BNNTs. As applying the electric field is one of the main methods to reduce the band gap of BNNTs, the effect of external electric field on the electronic properties of T-BNNTs and T-BC_2NNTs are also investigated.

2. Computational method

Our calculations are based on the density functional theory (DFT) method implemented in an OpenMX3.8 software package [62]. The generalized gradient approximation (GGA) with the representation of Perdew-Burke-Ernzerhof (PBE) is utilized to describe the electron exchange as well as correlation effects [63]. The tractable norm-conserving pseudopotential proposed by Morrison, Bylander, and Kleinman [64], which is a norm-conserving version of the ultrasoft pseudopotential by Vanderbilt [65] is used. The cutoff energy of the electronic wave function is 150 Ry. The electronic temperature is considered 300 K. All the considered tubes are optimized under periodic boundary conditions. The convergence tolerance is set to 0.001 eV/Å for the force. A vacuum separation exceeding 10 Å is incorporated to avoid interaction between adjacent nanotubes. Mulliken charge analysis is carried out to calculate the charge transfer between B, C, and N atoms.

For each tube, the cohesive energy, E_{coh}, is calculated as follows:

$$E_{coh} = (E_{Tube} - \sum_i n_i E_i) \Big/ \sum_i n_i \quad (1)$$

here, E_{Tube} is the total energy of the nanotube; E_i and n_i represent the energy and the number of isolated single i = B, C, and N atoms, respectively. According to this definition, a stable structure has negative cohesive energy, and more negative cohesive energy implies an energetically more favorable structure.

Ab initio molecular dynamics (AIMD) simulations are carried out to investigate the thermal stability of the tubes. All investigated structures are systematically thermalized for 5 ps with a time step of 1 fs at 300 K.

The dynamical stability of the sheets is examined by calculating frequencies of all phonon modes in Brillouin Zone (BZ) using the Siesta package [66].

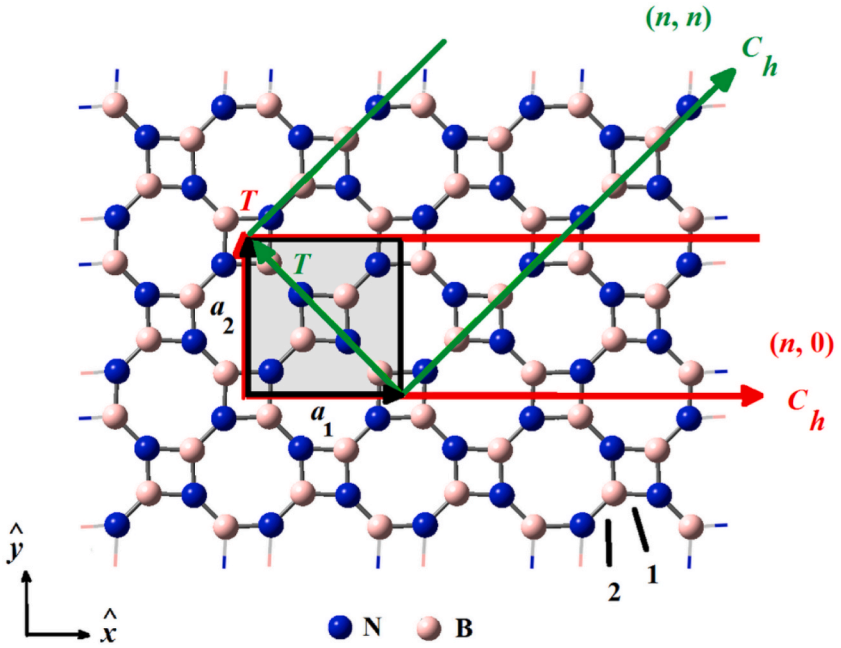

Fig. 1. Atomic structures of BN T-graphene sheet. $\vec{a}_1$ and $\vec{a}_2$ are lattice vectors of BN T-graphene sheet. $\vec{C}_h$ and $\vec{T}$ of $(n, 0)$ and (n, n) T-BNNTs are shown by red and green vectors.

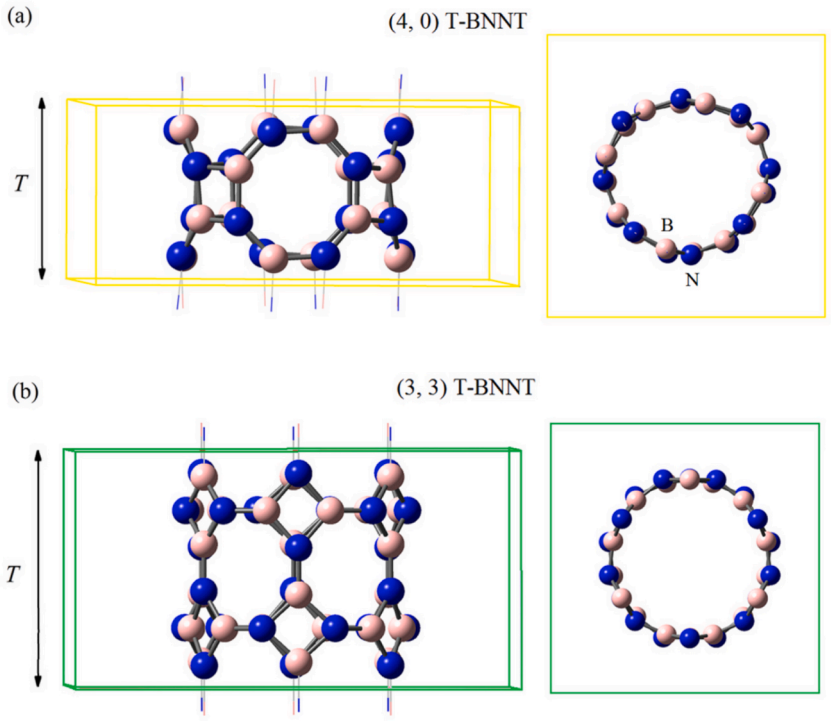

Fig. 2. Atomic structures of (a) (4, 0) and (b) (3, 3) T-BNNTs (Top and side views).

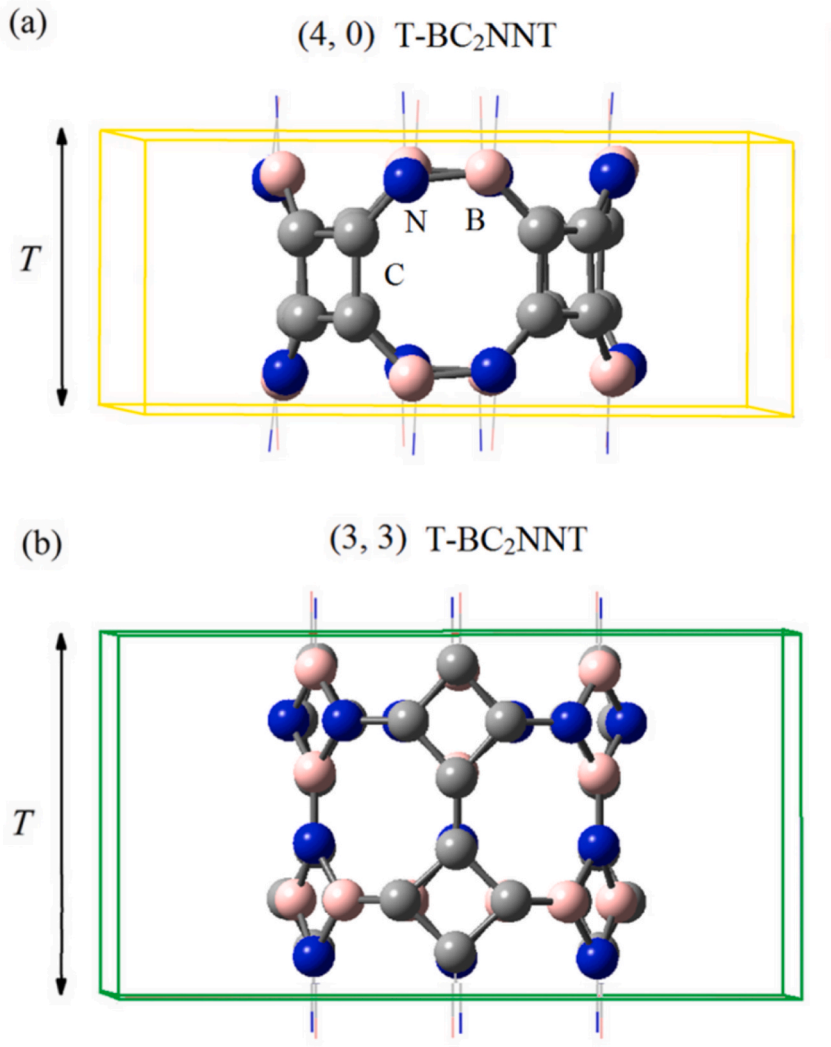

Fig. 3. Atomic structures of (a) (4, 0) and (b) (3, 3) T-BC_2NNTs (side view).

3. Results and discussion

3.1. Structure and stability of T-BNNTs and T-BC_2NTs

The atomic structure of a planar BN sheet with T-graphene structure that is formed from the tetragonal and octagonal rings periodically is illustrated in Fig. 1. The unit cell of the BN T-graphene sheet is highlighted by gray color, and it contains four B and four N atoms. Two types of B–N bonds exist: B–N bonds in the squares, and B–N bonds connecting the different squares. These bonds are labeled by 1 and 2 in Fig. 1, i.e B–N (1) and B–N (2). The optimized bond lengths of B–N (1) and B–N (2) are 1.46 and 1.43 Å, respectively.

Two sets of nanotubes have been constructed by rolling the BN T-graphene sheets in different directions. These tubes are called T-BNNTs. Similar to the ordinary CNTs, the chiral vector is defined as $\vec{C}_h = n\vec{a}_1 + m\vec{a}_2$, where $\vec{a}_1 = a\hat{x}$ and $\vec{a}_2 = a\hat{y}$ are primitive lattice vectors of the BN T-graphene sheet, and n and m are integer numbers. The chiral vector determines the circumferential and chirality of the tube. T-BNNTs of two different chiralities called (n, 0) and (n, n) tubes have been studied in this work: (n, 0) T-BNNTs with $n = 3$–16, and (n, n) T-BNNTs with $n = 2$–10. As an example, the atomic structures of (4, 0) and (3, 3) T-BNNTs are displayed in Fig. 2. First, the dimensions of the unit cell of (n, 0) and (n, n) T-BNNTs (named T in Fig. 1) are considered to be equal to a and $\sqrt{2}a$. The lengths of the tubes are optimized, where the optimized tube lengths are found to be 5.08 and 7.12 Å for (n, 0) and (n, n) T-BNNTs, respectively. In Fig. 1, C_h and T for (n, 0) and (n, n) tubes are shown by red and green vectors, respectively.

For (n, 0) T-BNNTs, the lengths of B–N (1) bond along the tube axis, B–N (1) bond perpendicular to the axis of the tube, and B–N (2) bond are 1.49, 1.47, 1.43 Å, respectively. The lengths of the bonds of B–N (1), and B–N (2) along the tube axis, and B–N (2)

Table 1
The bond lengths of (n, 0) and (n, n) T-BC_2NNTs. Here, (1) and (2) denotes the type of bonds as shown in Fig. 1 and (a) and (p) point to the bonds along and perpendicular to the tube axis, respectively.

	C–C	B–N	B–C	N–C
(n, 0)	1.53 (1a) 1.41 (1p)	1.50	1.50	1.40
(n, n)	1.48 (1) 1.42 (2)	1.50 (1) 1.39 (2)	1.50	1.35

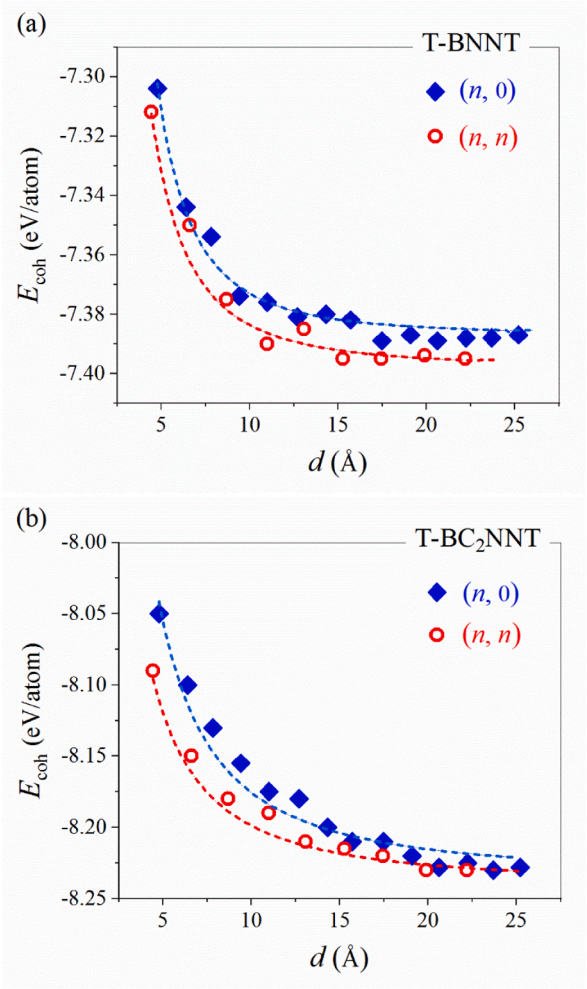

Fig. 4. Cohesive energy, E_{coh}, as a function of tube diameter, d.

perpendicular to the tube axis are 1.49, 1.42, 1.41 Å in (n, n) T-BNNTs, respectively. The B–N bond lengths of T-BNNTs are found to be close to those of the BN T-graphene sheet. The B–N bonds elongate parallel to the tube axis, whilst the B–N bonds shorten perpendicular to the axis of the tube.

The Mulliken charge analysis shows that all B atoms are positively charged, whilst N atoms are negatively charged. The charges on B and N atoms are +0.7 and −0.7 e, respectively. Hence, B atom loses an average of 0.7 electron charges, while N atom gains an average of this amount of charge when present in T-BNNTs because of charge transfer from the low electronegative B atoms to the highly electronegative N atoms. These results describe the ionic nature of bonds between B and N atoms.

The T-BC_2NNTs are obtained by substitution of B and N atoms of T-BNNTs with C atoms. As B and N atoms in BCN structures prefer to occupy adjacent sites [32,60], T-BC_2NNTs which each BN pair replaces two adjacent C atoms of T-BNNTs are considered. For (n, 0) and (n, n) T-BC_2NNTs, four and three configurations with different arrangements of atoms are constructed. The total energy of tubes is compared to determine the most favorable configuration. For instance, the energetically most favorable configurations of (4, 0) and (3, 3) T-BC_2NNTs are shown in Fig. 3. The bond lengths of (n, 0) and (n, n) T-BC_2NNTs are listed in Table 1.

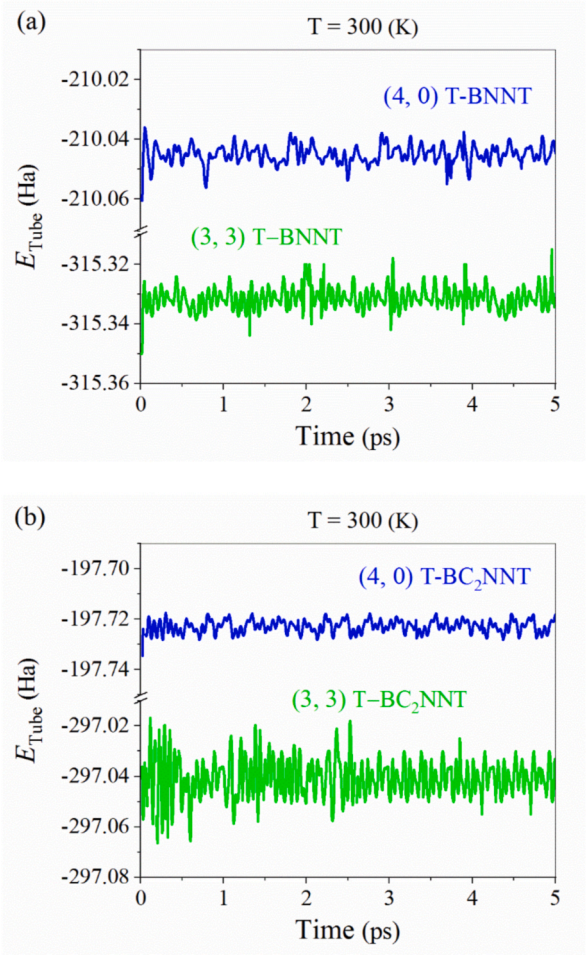

Fig. 5. Fluctuation of total energy, E_{Tube}, of (4, 0) and (3, 3) T-BNNTs and T-BC_2NNTs versus the simulation time at 300 K.

In T-BC_2NNTs similar to T-BNNTs, all B and N atoms are positively and negatively charged, respectively. The charge on B atoms is +0.34 e, and the charge on N atoms is −0.64 e. The C atoms gain −0.03 e from B atoms in their neighboring because B atoms have lower electronegativity than C atoms. While, charges of 0.33 e transfer from C atoms to N in their neighboring because of charge transfer from C atoms with lower electronegativity to N atoms with higher electronegativity.

As the stability of a structure is characterized by interatomic bond energy, the cohesive energy of T-BNNTs and T-BC_2NNTs is calculated. The dependence of the cohesive energy of T-BNNTs and T-BC_2NNTs on the tube diameter is presented in Fig. 4. Here, the cohesive energy estimates the possibility of the experimental synthesis of the suggested nanotubes, where negative cohesive energy means that the formation of T-BNNTs and T-BC_2NNTs is an exothermic process. The (n, n) nanotubes are more stable than (n, 0) ones for similar diameters. The results indicate that T-BC_2NNTs are more stable than T-BNNTs. The cohesive energy turns further negative with enlarging the diameter of T-BNNTs and T-BC_2NNTs similar to nanotubes based on: graphene, S-graphene, graphyne, as well as nitrogenated holey graphene sheets [54–57,60]. A suitable fitting function that defined the relation between the cohesive energy and the diameter is determined by curve fitting tools in Origin package [67]. It is found that the data match by a power law of $\frac{1}{d^x}$, where d denotes the tube diameter. Here, x is 2.44 for (n, 0) and 2.20 for (n, n) T-BNNTs. In (n, 0) and (n, n) T-BC_2NNTs, x is 1.60 and 1.52, respectively. Hence, the stability of T-BNNTs and T-BC_2NNTs increases as their diameter increases. When the diameter is sufficiently large, the cohesive energy of the considered T-BNNTs and T-BC_2NNTs nanotubes converges to −7.39 and −8.23 eV/atom, i.e the cohesive energy of the BN and BC_2N T-graphene sheets. These suggest that large diameter T-BNNTs and T-BC_2NNTs are as stable as BN and BC_2N T-graphene sheets.

Furthermore, AIMD simulation is performed to investigate the thermal stability of T-BNNTs and T-BC_2NNTs at 300 K for 5 ps The results of AIMD simulations indicate that all structures are well preserved without apparent distortion or collapse. No sign of structural instability is detected for T-BNNTs and T-BC_2NNTs by the AIMD simulations. For example, total energy fluctuations as a function of simulation time at 300 K of the (4, 0) and (3, 3) T-BNNTs and T-BC_2NNTs are illustrated in Fig. 5. The fluctuation of total energy around certain average values is observed for the entire AIMD simulation. Since the structures stay intact at room temperature with stable energy, one can conclude that the T-BNNTs and T-BC_2NNTs exhibit desirable thermal stability.

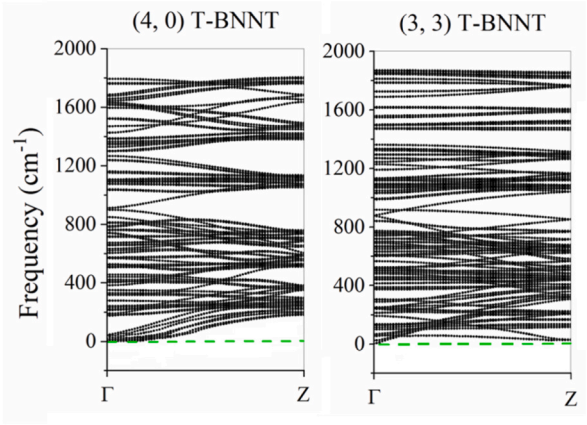

Fig. 6. Phonon spectra for (4, 0) and (3, 3) T-BNNTs.

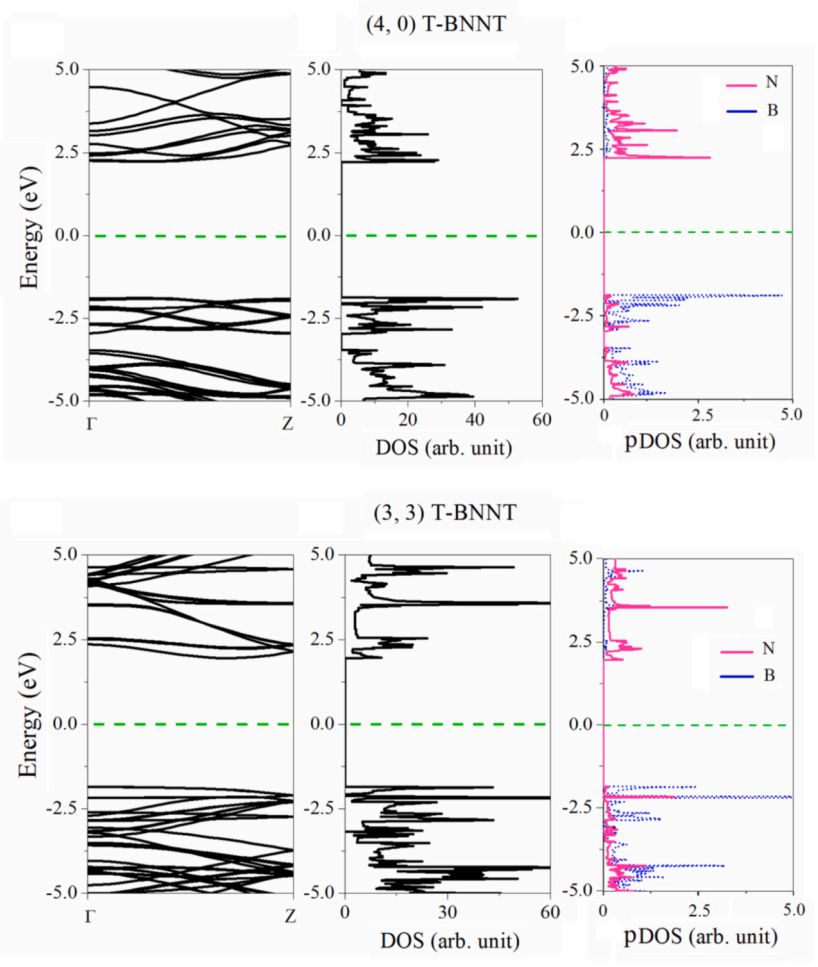

Fig. 7. Electronic band structure, DOS, and pDOS of (4, 0) and (3, 3) T-BNNTs. (The Fermi level is located at 0 eV)

To search the dynamic stability of the tubes, the phonon dispersion is calculated. As an example, the phonon dispersion curves of the (4, 0) and (3, 3) T-BNNTs are shown in Fig. 6. Here, the phonon branches are free from imaginary frequencies throughout the whole BZ. Similar results are observed for other tubes. Hence, the considered tubes are stable dynamically.

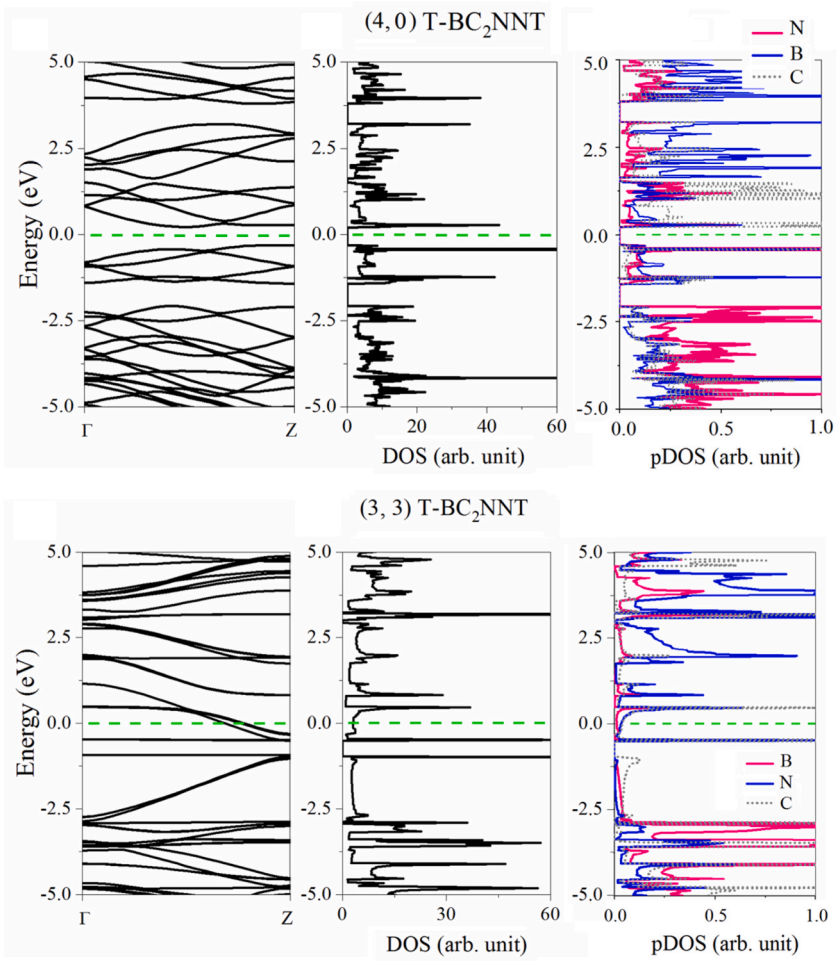

Fig. 8. Electronic band structure, DOS, and pDOS of (4, 0) and (3, 3) T-BC_2NNT. (The Fermi level is located at 0 eV)

3.2. *Electronic properties of T-BNNTs and T-BC_2NNTs*

To study the electronic properties of T-BNNTs and T-BC_2NNTs, the electronic band structures and DOS of the nanotubes are evaluated. The electronic band structure, DOS, and partial DOS (pDOS) of (4, 0) and (3, 3) T-BNNTs and T-BC_2NNTs are shown in Figs. 7 and 8. The Fermi energy is shifted to zero in all figures. For (4, 0) and (3, 3) T-BNNTs and (4, 0) T-BC_2NNTs, the maximum and minimum of valence and conduction bands do not overlap, and DOS is zero at the Fermi level. Hence, these tubes have semiconducting properties. In (3, 3) T-BC_2NNT, the valence and conduction bands overlap and DOS is non-zero at the Fermi level. Thus, (3, 3) T-BC_2NNT is a metal. A gap of 0.41 eV is observed at about 0.5 eV below the Fermi level. A similar band gap below the Fermi level is observed in T-BC_2N sheet [32]. With increasing the diameter of (n, n) T-BC_2NNT, this gap decreases and finally disappears when n becomes more than 5. It is obvious from the pDOS of T-BNNTs that the lowest unoccupied state is mainly formed by B atoms and the highest occupied state is mainly contributed by N atoms. In addition to B and N atoms, C atoms play a crucial role in forming the states near the Fermi level of T-BC_2NNTs. pDOS of T-BNNTs and T-BC_2NNTs are the same as that of T-BNNTs and T-BC_2N sheets [32,60,68].

The results indicate that all considered (n, 0) and (n, n) T-BNNTs, and (n, 0) T-BC_2NNTs in this work have semiconducting properties. The electronic properties of T-BNNTs and T-BC_2NNTs are very different from T-CNTs that have metallic or semimetallic properties [59]. It is well-known that the band gap of BN systems is assigned to the strong ionicity of B–N bonds [69–71]. The energy band gap of T-BNNTs and T-BC_2NNTs as a function of tube size is illustrated in Fig. 9. (The energy band gaps of all tubes are also listed in Table S1 of the supplementary file.) It can be seen that the band gap of the small T-BNNTs and T-BC_2NNTs is sensitive to the size and chirality of the tube. With increasing the tube diameter, the band gaps of the (n, 0) and (n, n) T-BNNTs change and converge to 3.97 and 3.86 eV, respectively. These values are close to the band gap of BN T-graphene sheet (4.00 eV) [32,72]. The band gaps of the (n, 0) T-BC_2NNTs with $n > 10$ decreases to 0.0 eV by increasing the tube diameter. Hence, the large T-BC_2NNTs show metallic properties. Such behavior is due to the competition between the size effect and the overlapping of π orbitals [73,74]. For the small tubes, a strong hybridization effect occurs because of the large curvature of the tubes [70,75]. The curvature effect and hybridization significantly modify the band structure and causes the band gap of the tube different from that of the sheet. With an increase in the tube diameter

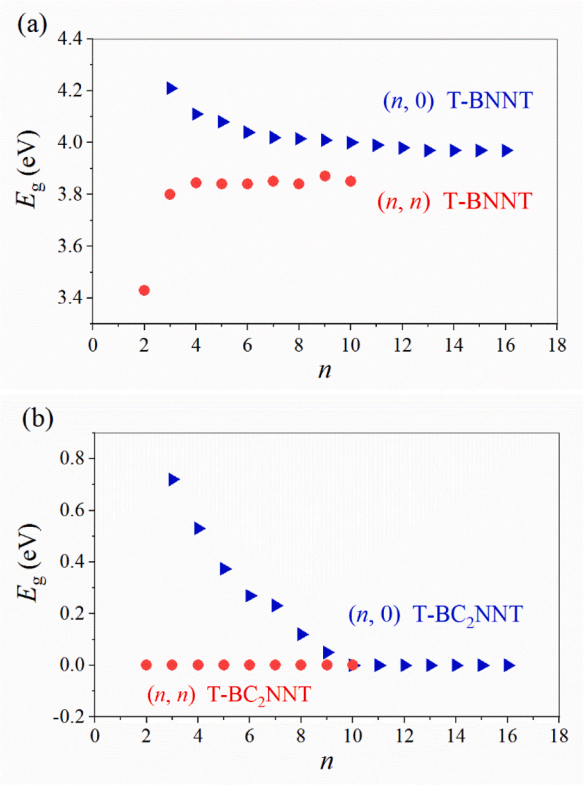

Fig. 9. Energy band gap, E_g, of (a) (n, 0) and (n, n) T-BNNTs, and (b) (n, 0) T-BC_2NNT as a function of tube size, n.

and a simultaneous decrease in the overlap, the band gap systematically changes with diameter due to the size effects. After saturation of the size effects, overlap remains but decreases with tube diameter. The energy gap reaches the value for plane monolayer, when the tube diameter is large enough to reduce the curvature hybridization effect to a constant minimum [73,74]. Therefore, the band gap of a tube with a large diameter eventually remains unchanged, about the band gap of the sheet [55–60,71].

The (n, 0) and (n, n) T-BNNTs, and (n, 0) T-BC_2NNTs exhibit insulators and semiconducting behavior with a band gap that is smaller than the band gap for graphene-like BN sheet and conventional BNNTs. This endows T-BNNTs and T-BC_2NNTs with more electronic applications as compared with the hexagonal BN sheet and nanotubes. Furthermore, the large T-BNNTs and T-BC_2NNTs with a relatively uniform band gap could be used in solar cells and digital switches without the need of chirality and radius sorting as is needed for devices based on CNTs.

3.3. *Effect of electric field*

The effect of an external electric field on the electronic properties of T-BNNTs and T-BC_2NNTs is explored by examining changes in their electronic band structures and DOS. An electric field, up to 1.0 V/Å, is applied perpendicular to the tube axis. As the external field is applied, the crossed or almost degenerated states in both the valence and conduction bands split. The bottom of the conduction band and the top of the valence band move close to each other and cause a reduction in the band gap. This is due to the perturbation induced by the external electric field which breaks the symmetry of the electronic states and mixes the sub-bands. The dependence of the energy band gap of (4, 0) and (3, 3) T-BNNTs, and (4, 0) T-BC_2NNTs on the external electric field is shown in Fig. 10. The band gaps of these tubes decrease as the electric field increases. With increasing the electric field strength, the modification of the band structure and consequently reduction of the band gap becomes further obvious. This sensitive response of T-BNNTs and T-BC_2NNTs to the external electric field would have potential applications in nanoelectronic devices that require variable electrical conductivity. For instance, they could be used as the tunneling channels for tunneling field effect transistors because they conduct current only if sufficient bias voltages are applied.

4. Conclusions

The structural as well as electronic properties of BN and BC_2N nanotubes with a structure of T-graphene structure (T-BNNTs and T-BC_2NNTs) are studied by density functional theory (DFT). The structural stability, electronic band structure, along with density of states of (n, 0) and (n, n) T-BNNTs and T-BC_2NNTs with different sizes are systematically studied. The cohesive energy was found to be

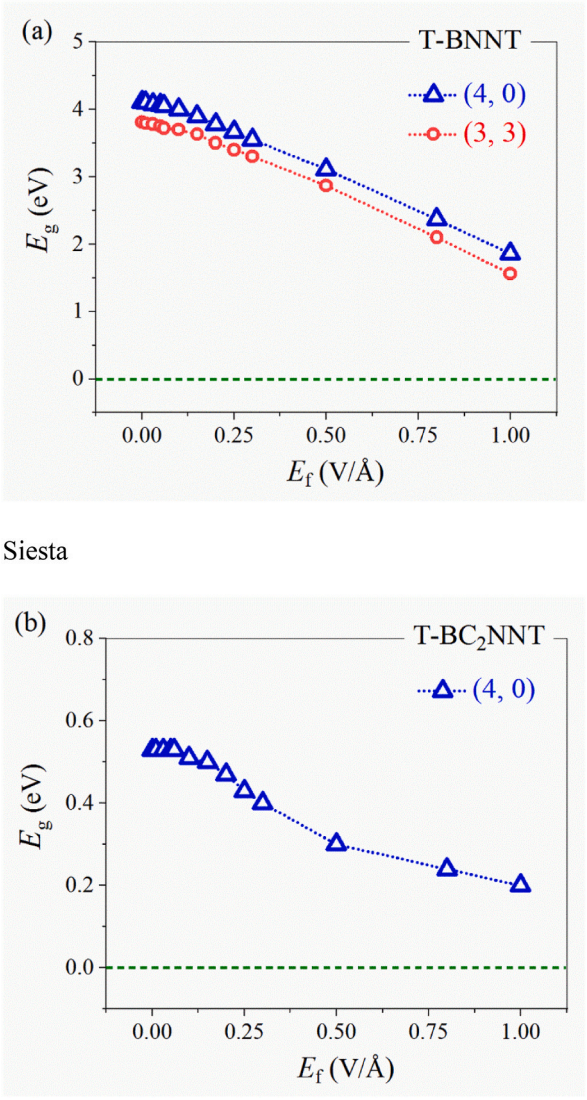

Fig. 10. Energy band, E_g, as a function of the applied electric field, E_f, for (a) (4, 0) and (3, 3) T-BNNTs and (b) (4, 0) T-BC_2NNT.

negative for these tubes, which denotes that the formation of the tubes is an exothermic reaction. It is found that T-BC_2NNTs present higher stability than T-BNNTs. Ab-initio molecular dynamics simulations and phonon calculations reveal the thermal and dynamical stability of the considered nanotubes at room temperature. The band gap calculations indicate that all T-BNNTs and (n, 0) T-BC_2NNTs behave as insulators and semiconductors, while (n, n) T-BC_2NNTs show metallic properties. The band gap of T-BC_2NNTs is smaller than those of T-BNNTs. T-BNNTs with large diameters show almost constant band gap which is independent of the chirality and diameter. The large diameter T-BC_2NNTs behave as metals. Hence, it is not essential to control the chirality and diameter of these tubes to use in electronic devices. Applying an external electric field decreases the band gap energy. It can conclude that the T-BNNTs and T-BC_2NNTs are stable and exhibit tunable band gap energy that can be used for nanosized electronic and photonic device applications that require adjustable conductivity.

Author statement

Roya Majidi conceived of the presented idea, performed the computations, and prepared draft manuscript. **Ahmad I. Ayesh** reviewed the results and prepared the final version of the manuscript.

Declaration of competing interest

The authors declare that they have no known competing financial interests or personal relationships that could have appeared to

influence the work reported in this paper.

Acknowledgement

The work was supported by Shahid Rajaee Teacher Training University.

Appendix A. Supplementary data

Supplementary data to this article can be found online at https://doi.org/10.1016/j.micrna.2022.207244.

References

[1] K.S. Novoselov, A.K. Geim, S.V. Morozov, D. Jiang, Y. Zhang, S.V. Dubonos, I.V. Grigorieva, A.A. Firsov, Science 306 (2004) 666.
[2] F. Schweirz, Nat. Nanotechnol. 5 (2010) 487.
[3] A.A. Baladin, Nat. Mater. 10 (2011) 569.
[4] A.G. Olabi, M.A. Abdelkareem, T. Wilberforce, E.T. Sayed, J. Renew. Sustain. Energy 135 (2021) 110026.
[5] S. Sato, Jpn. J. Appl. Phys. 54 (2015), 040102.
[6] K.S. Novoselov, A.K. Geim, S.V. Morozov, D. Jiang, Y. Zhang, S.V. Dubonos, I.V. Grigorieva, A.A. Firsov, Science 306 (2004) 666.
[7] A.K. Geim, K.S. Novoselov, Nat. Mater. 6 (2007) 183.
[8] C. Lee, X.D. Wei, J.W. Kysar, J. Hone, Science 321 (2008) 385.
[9] M.Z. Hasan, J.E. Moore, Annu. Rev. Conden. Mat. P. 2 (2011) 55.
[10] K.S. Novoselov, A.K. Geim, S.V. Morozov, et al., Nature 438 (2005) 197.
[11] N.O. Weiss, H. Zhou, L. Liao, et al., Adv. Mater. 24 (2012) 5782.
[12] Y.B. Zhang, Y.W. Tan, H.L. Stormer, et al., Nature 438 (2005) 201.
[13] K.I. Bolotin, K.J. Sikes, Z. Jiang, et al., Solid State Commun. (2008) 351.
[14] Y. Liu, Q. Huang, L. Guo, X. Chen, Phys. Rev. Lett. 108 (2012) 1.
[15] S. Nath, A. Bandyopadhyay, S. Datta, M.M. Uddin, D. Jana, Physica E 120 (2020) 114087.
[16] W.J. Yin, Y.E. Xie, L.M. Liu, R.Z. Wang, X.L. Wei, L. Lau, J.X. Zhong, Y.P. Chen, J. Mater. Chem. 1 (2013) 15341.
[17] S. Das, D. Sen, K.K. Chattopadhyay, J. Phys. Chem. Chem. Phys. 18 (2016) 2494.
[18] R.H. Baughman, H. Eckhardt, M. Kertesz, J. Chem. Phys. 87 (1987) 6687.
[19] S. Zhang, J. Zhou, Q. Wang, X. Chen, Y. Kawazoe, P. Jena, Proc. Natl. Acad. Sci. Unit. States Am. 112 (2015) 2372.
[20] Z. Wang, X.F. Zhou, X. Zhang, Q. Zhu, H. Dong, M. Zhao, A.R. Oganov, Nano Lett. 9 (2015) 6182.
[21] J. Wang, F. Ma, M. Sun, RSC Adv. 7 (2017) 16801.
[22] J. Jung, A.M. DaSilva, A.H. MacDonald, S. Adan, Nat. Commun. 6 (2015) 6308.
[23] M. Xum, T. Liang, M. Shi, H. Chen, Chem. Rev. 113 (2013) 3766.
[24] J.Y. Dai, P. Giannozzi, J.M. Yuan, Surf. Sci. 603 (2009) 2328.
[25] Y. Kubota, K. Watanabe, O. Tsuda, T. Taniguchi, Science 317 (2007) 932.
[26] J.Y. Dai, J.M. Yuan, Phys. Rev. B 81 (2010) 165414.
[27] S.H. Mir, S.H. Mir, V.K. Yadav, J.K. Singh, ACS Omega 4 (2019) 3732.
[28] K. Watanabe, T. Taniguchi, H. Kanda, Nat. Mater. 3 (2004) 404.
[29] O. Hod, J. Chem. Theor. Comput. 8 (2012) 1360.
[30] N. Zhang, X. Wu, Chin. J. Chem. Phys. 27 (2014) 394.
[31] R. Majidi, T. Rabczuk, J. Phys. Chem. Solid. 139 (2019) 109115.
[32] R. Majidi, Physica E 74 (2015) 371.
[33] J. Siqia, Y. Shashaa, W. Xiaoa, W. Gub, Mol. Phys. 118 (2020), e1757775.
[34] T. Zhai, J. Yao, One-Dimensional Nanostructures: Principles and Applications, Wiley Online Library, Print, 2012, ISBN 9781118071915, https://doi.org/10.1002/9781118310342. Online ISBN: 9781118310342.
[35] H. Dai, Surf. Sci. 500 (2002) 218.
[36] R.H. Baughman, A.A. Zakhidov, W.A. de Heer, Science 297 (2002) 787.
[37] M.M. Rana, D.S. Ibrahim, M.R. Mohd Asyraf, S. Jarin, A. Tomal, Sens. Rev. 37 (2017) 127.
[38] M. Fazilaty, M. Pouradmadi, M.R. Shayesteh, S. Hashemian, J. Phys. Chem. Solid. 148 (2020) 10963.
[39] V. Schroeder, S. Savagatrup, M. He, S. Lin, T.M. Swager, Chem. Rev. 119 (2019) 599.
[40] D. Golberg, Y. Bando, Y. Huang, T. Terao, M. Mitome, C. Tang, C. Zhi, ACS Nano 4 (2010) 2979.
[41] M. Cohen, A. Zettl, Phys. Today 63 (2010) 34.
[42] X. Blase, A. Rubio, S.G. Louie, M.L. Cohen, EPL-EuroPhys. Lett. 28 (1994) 335.
[43] K. Nejat, E. Vessally, P. Delir Nezhad, H. Mofid, A. Bekhradnia, J. Phys. Chem. Solid. 111 (2017) 238.
[44] S.D. Dabhi, P.K. Jha, Mater. Res. Express 3 (2016), 085015.
[45] F. Gomes, V. Dmitriev, C. Nascimento, J. Microw. Optoelectron. Electromagn. Appl. 13 (2014) 214.
[46] A. Bahari, A. Jalalinejad, M. Bagheri, M. Amiri, Solid State Commun. 189 (2014) 1.
[47] A. Bahari, A. Jalalinejad, M. Bagheri, M. Amiri, Solid State Commun. 267 (2017) 1.
[48] Z. Weng-Sieh, K. Cherrey, N.G. Chopra, X. Blase, Y. Miyamoto, A. Rubio, M.L. Cohen, S.G. Louie, A. Zettl, R. Gronsky, Phys. Rev. B 51 (1995) 11.
[49] K. Suenaga, C. Colliex, N. Demoncy, A. Loiseau, H. Pascard, F. Willaime, Science 278 (1997) 653.
[50] H. Pan, Y.P. Feng, J. Lin, Nanoscale Res. Lett. 4 (2009) 498.
[51] P. Nematollahi, M.D. Esrafili, E.C. Neyts, Surf. Sci. 39 (2018) 672.
[52] D. Zhang, S. Zhangm N. Yapici, R. Oakley, S. Sharma, V. Parashar, Y.K. Yap, ACS Omega 6 (2021) 20722.
[53] L. Li, W. Qiao, H. Bai, Y. Huang, RSC Adv. 10 (2020) 16709.
[54] A.I. Kochaev, R.M. Meftakhutdinov, R.T. Sibatov, D.A. Timkaeva, Comput. Mater. Sci. 186 (2021) 109999.
[55] M. BabaeiPoura, E. Keshavarz Safaria, A.A. Shokrib, Physica E 86 (2017) 129.
[56] R. Majidi, Diam. Relat. Mater. 118 (2021) 108520.
[57] R. Majidi, J. Electron. Mater. 47 (2018) 2890.
[58] R. Majidi, M. Odelius, Sh AlTaha, Diam. Relat. Mater. 82 (2018) 96.
[59] L.H. Xu, J.Q. Hu, J.H. Zhang, S.Q. Wu, F.C. Chuang, Z.Z. Zhu, K.M. Ho, New J. Phys. 21 (2019) 53015.
[60] F. Li, J. Lu, H. Zhu, X. Lin, Res. Phys. 9 (2018) 656.

[61] F. Li, J. Lu, G. Tan, M. Ma, X. Wang, H. Zhu, Phys. Lett. A 383 (2019) 76.
[62] T. Ozaki, H. Kino, J. Yu, M.J. Han, N. Kobayashi, M. Ohfuti, F. Ishii, et al., User's Manual of OpenMX Version 3.8, http://www.openmx-square.org.
[63] J.P. Perdew, K. Burke, M. Ernzerhof, Phys. Rev. Lett. 77 (1996) 3865.
[64] I. Morrison, D.M. Bylander, L. Kleinman, Phys. Rev. B 47 (1993) 6728.
[65] D. Vanderbilt, Phys. Rev. B 41 (1990) 7892.
[66] J.M. Soler, E. Artacho, J.D. Gale, A. Garcia, J. Junquera, P. Ordejon, D. Sanchez-Portal, J. Phys. Condens. Matter 14 (2002) 2745.
[67] www.originlab.com.
[68] C. Yao, Y. Tang, D. Liu, H. Zhu, Superlattice. Microst. 92 (2016) 198.
[69] M. Topsakal, E. Akturk, S. Ciraci, Phys. Rev. B 79 (2009) 115442.
[70] C.H. Park, S.G. Louie, Nano Lett. 8 (2008) 2200.
[71] A. Rubio, J.L. Corkill, M.L. Cohen, Phys. Rev. B 49 (1994) 5081.
[72] M. Shahrokhi, B. Mortezavi, G.R. Berdiyorovc, Solid State Commun. 253 (2017) 51.
[73] H. Pan, Y.P. Feng, J.Y. Lin, Phys. Rev. B 73 (2006), 035420.
[74] S. Azevedo, R. de Paiva, J.R. Kaschny, J. Phys. Condens. Matter 18 (2006) 10871.
[75] X. Blasé, A. Rubio, S.G. Louie, M.L. Cohen, Europhys. Lett. 28 (1994) 335.